UC Irvine
UC Irvine Previously Published Works

Title

Description and characterization of the complex modes in a linear chain of gold nanospheres

Permalink

https://escholarship.org/uc/item/2th7p7c5

ISBN

9780819484833

Authors

Campione, Salvatore
Steshenko, Sergiy
Capolino, Filippo

Publication Date

2011-02-10

DOI

10.1117/12.873957

Peer reviewed

Description and characterization of the complex modes in a linear chain of gold nanospheres

Salvatore Campione[a], Sergiy Steshenko[b,c], Filippo Capolino*[a]

[a]Dept. of Electrical Engineering and Computer Science, University of California, Irvine, CA 92697-2625, USA

[b]Dept. of Information Engineering, University of Siena, 53100 Siena, Italy

[c]Institute of Radiophysics and Electronics of the National Academy of Sciences of Ukraine, 61085, Kharkiv, Ukraine

ABSTRACT

In this paper, complex modes in a linear chain of gold nanospheres are analyzed, accounting for metal losses. Dispersion diagrams are computed for travelling modes with both longitudinal and transverse (with respect to the array axis) polarization states. The procedure outlined in this work allows for the description of single mode evolution varying frequency, thus the modal dispersion diagrams are composed by the superposition of all the different modes in the one dimensional array. Each nanoparticle is modeled as an electric dipole, by adopting the single dipole approximation, and the complex zeroes of the homogeneous equation characterizing the field in the periodic structure are computed. The Ewald method is employed to analytically continue the periodic Green's function into the complex spectral domain and to achieve rapid convergence. Full characterization of the modes is provided in terms of their direction of propagation (forward/backward), their guidance and radiation properties (bound/leaky), the position of their wavenumber on the Riemann sheet (proper/improper), and also in terms of their possible physical excitation in the structure by a source in proximity of the array or a defect (physical/nonphysical modes). Understanding the modes excitable in this kind of structures is essential for possible applications in which the linear chain can be employed, from near-field enhancement to SERS, and innovative sensors.

Keywords: nanospheres, linear chains, plasmonics, mode analysis, metamaterials.

1. INTRODUCTION AND STATEMENT OF THE PROBLEM

Periodic arrays of plasmonic nanospheres have been recently adopted in several applications in the optical field (near-field enhancement and super-resolution [1-5]), in the directive radiation [6], and in the biological and chemical fields (microscopy and spectroscopy using SERS [7-8], biosensors [9-10], DNA detectors [11]). However, despite these applications in which these arrays could be used, it is still quite hard to fully control and determine characteristics with a particular set of excitation wavelengths. Indeed, several difficulties are still encountered in the analysis and interpretation of mode propagation in 1D- and 2D-periodic arrays of metallic nanospheres. The evolution and the interactions between different modes are still unclear, and based on what it has been published so far it is somehow hard to discern if a mode is physical or not. These are the reasons why it is important to perform a thorough mode analysis for this kind of arrays.

In this paper we present and interpret dispersion diagrams for linear chains of gold nanospheres. The reader is referred to [12-14] and references therein for detailed theoretical physical explanations and for a list of state of the art work not reported here for the sake of brevity. In the particular case of linear chains of plasmonic nanospheres, in [12-13], the numerical results were relevant to the case of silver nanospheres. In this paper, instead, we consider the case of gold nanospheres shown in Fig. 1. As described in the following sections, gold losses are larger than those of silver, the high frequency parameter of gold almost doubles the silver one and the gold plasma frequency is slightly smaller than the silver one, resulting in different modal dispersion diagrams for the chain.

*f.capolino@uci.edu; phone 1 949-824-2164; http://capolino.eng.uci.edu/

The structure of the paper is as follows. The mathematical description for the simulation model adopted to perform the analyses described in this paper is briefly summarized in Sec. 2. The dispersion diagrams comprising complex bound and leaky modes in linear chains of gold nanospheres are reported in Sec. 3, considering the presence of losses in the nanoparticles, for both transversal and longitudinal polarization states. The physical interpretation of the obtained results in terms of guidance and radiation, and physical excitation, is provided as well. Conclusions are in Sec. 4.
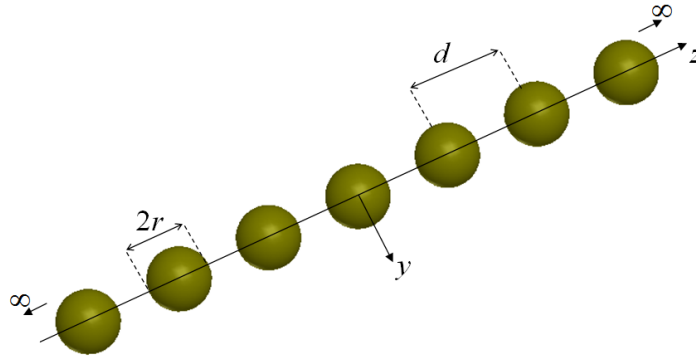

Fig. 1. Linear chain of gold nanospheres, of infinite extent, periodic along the z-direction, embedded in a homogeneous medium with permittivity ε_h. r is the radius of each nanoparticle, and d is the center-to-center distance (periodicity). The reference system shown here will be adopted throughout the paper.

2. FORMULATION

The aim of this section is to briefly describe the formulation adopted to perform mode analysis in a linear chain of metallic nanospheres, and the criteria for determining physical bound and leaky waves. A more detailed formulation and explanation is in [12-13,15]. Notice that the formulation outlined here is general, and is adopted in the following sections to characterize a particular array case.

2.1 Definition of the simulation model

The formulation is based on the single dipole approximation (SDA) [15-16]. According to SDA, each plasmonic nanosphere of the linear chain, at optical frequencies, acts as a single-dipole and can be described by a polarization vector

$$\mathbf{p} = \alpha_e \mathbf{E}^{loc}, \tag{1}$$

where α_e is the electric polarizability of the nanosphere, and $\mathbf{E}^{loc}$ is the local field produced by all the nanoparticles of the array except the considered nanoparticle plus the external incident field to the array [13,15].

The value of the polarizability α_e of a nanoparticle depends on both its geometry and material properties [15,17-18]. Here, we assume that α_e is obtained according to Mie theory [13,15-16,19-20], as shown for example in eq. (8.9) in [15] or in chapter 4 in [16].

The monochromatic time harmonic convention, $\exp(-i\omega t)$, is assumed and is therefore suppressed hereafter. Furthermore, the relative permittivity of the metal of each nanosphere is described by the Drude model

$$\varepsilon_m = \varepsilon_\infty - \frac{\omega_p^2}{\omega(\omega + i\gamma)}, \tag{2}$$

where ε_∞ is a high-frequency fitting parameter, ω_p is the plasma frequency of the metal (expressed in rad/s) and γ is the damping factor (expressed in s^{-1}).

Consider now a linear chain of nanospheres, for which each nanoparticle is placed at position $z_n = nd$, with $n = 0, \pm 1, \pm 2, \ldots$, and d is the period of the chain. Suppose that the array is immersed in a homogeneous background, with relative permittivity ε_h, and that the array is then excited by a plane wave or by a quasi-periodic excitation with wavevector $\mathbf{k}_B = k_z \hat{\mathbf{z}}$ [15]. Consequently, each nanoparticle will have a dipole moment equal to $\mathbf{p}_n = \mathbf{p}_0 e^{ink_z d}$. Then, the local field acting on a nanosphere at position $z_0 = 0$ is given by

$$\mathbf{E}^{\text{loc}}(k_z) = \mathbf{E}^{\text{inc}}(k_z) + \underline{\breve{\mathbf{G}}}^{\infty}(k_z) \cdot \mathbf{p}_0, \tag{3}$$

where $\underline{\breve{\mathbf{G}}}^{\infty}(k_z)$ represents the regularized electric-field dyadic Green's function for the phased period array of nanoparticles, that provides the field contribution of all the nanospheres but the one at position $z_0 = 0$.

Substituting then the expression for the local field given in (3) into (1), it follows that

$$\mathbf{p}_0 = \alpha_e \left[\mathbf{E}^{\text{inc}}(k_z) + \underline{\breve{\mathbf{G}}}^{\infty}(k_z) \cdot \mathbf{p}_0 \right], \tag{4}$$

which leads to the linear system

$$\underline{\mathbf{A}}(k_z) \cdot \mathbf{p}_0 = \mathbf{E}^{\text{inc}}(k_z), \qquad \underline{\mathbf{A}}(k_z) = \frac{1}{\alpha_e} \mathbf{I} - \underline{\breve{\mathbf{G}}}^{\infty}(k_z). \tag{5}$$

The dyadic Green's function $\underline{\breve{\mathbf{G}}}^{\infty}(k_z)$ is computed by using the Ewald's method, which provides two series with Gaussian convergence and only a handful of terms are needed [21-23].

The mode dispersion analysis in the linear chain is then obtained by computing the complex k_z-zeroes of the homogeneous linear system in (5), after having imposed no excitation source (i.e., $\mathbf{E}^{\text{inc}}(k_z) = 0$). Therefore, the complex zeros of the determinant of $\underline{\mathbf{A}}(k_z)$ have to be computed.

2.2 Definition of Floquet spatial harmonics

The electric field in the linear chain, due to the periodicity of the array, is quasi-periodic, i.e., it is periodic except for an inter-element phase shift. Thus, it can be described as $\mathbf{E}(\mathbf{r} + d\hat{\mathbf{z}}, k_z) = \mathbf{E}(\mathbf{r}, k_z) e^{ik_z d}$, where d is the period of the periodic structure, $k_z = \beta_z + i\alpha_z$ is the wavenumber along the array axis, and $\mathbf{r} = x\hat{\mathbf{x}} + y\hat{\mathbf{y}} + z\hat{\mathbf{z}}$. A mode in the linear chain is expressed in term of a Fourier series expansion, and thus represented as the superposition of Floquet spatial harmonics

$$\mathbf{E}^{\text{mode}}(\mathbf{r}, k_z) = \sum_{p=-\infty}^{\infty} e^{ik_{z,p} z} \mathbf{e}_p^{\text{mode}}(x, y, k_z), \tag{6}$$

where $k_{z,p} = k_z + 2\pi p / d = \beta_{z,p} + i\alpha_z$, with p the order of the Floquet spatial harmonic, and $\mathbf{e}_p$ is the weight of the p-th harmonic. For more details, the reader is referred to [12-13] and references therein.

2.3 Definition of physical modes

The physical modes that can be excited in linear chains of plasmonic nanospheres are summarized in Table 1 in [12], in Table 12.1 in [14] or in [24]. To be physical, a mode has to have a complex wavenumber, i.e., a complex value representing a zero of the determinant of $\underline{\mathbf{A}}(k_z)$, that is captured in the integration path outlined in [12-14,25]. Looking at the positive z-direction, in order to be captured in the path deformation, a complex wavenumber $k_z = \beta_z + i\alpha_z$ should have $\alpha_z \geq 0$. Moreover, to be physical, not only it needs to have $\alpha_z \geq 0$, but also it has to respect the conditions stated in the following. As such, considering the modal harmonic in the fundamental Brillouin zone (BZ), a physical forward wave belongs to the I quadrant of the complex k_z plane, whereas a backward one to the II quadrant. Looking at a positive z-direction, k_z wavenumbers in the II quadrant representing backward proper (i.e., belonging to the top

Riemann sheet) waves (either bound or leaky) are physical; whereas in the leaky region of the I quadrant (i.e., above the light line in the $k\beta$-plane), wavenumbers representing forward improper (i.e., belonging to the bottom Riemann sheet) leaky waves are physical; last, wavenumbers in the bound region of the I quadrant of the complex k_z plane (i.e., below the light line in the $k\beta$-plane) are physical forward proper bound waves. For more details about physical conditions, path deformation and proper/improper Riemann sheets, the reader is referred to [12-14] and references therein.

2.4 Definition of bound and leaky modes

A *bound mode* is a physical mode that has *all* its Floquet wavenumbers outside the visible region, or $\left|\beta_{z,p}\right| > k$, where $k = k_0\sqrt{\varepsilon_h}$ is the wavenumber in the homogeneous background (host wavenumber), and k_0 is the free space wavenumber. Taking into account of the physical condition in Sec. 2.3, and considering the harmonic in the first BZ, an observer along the positive *z*-direction would be reached by a mode (excited at the origin) either when (i) it is proper (top Riemann sheet of the complex k_z plane) and $k < \beta_z$ and α_z is positive (forward mode), or when (ii) it is proper and $\beta_z < -k$ and α_z is positive (backward mode). It can be noticed that physical waves for positive *z*-direction are limited to the first and second quadrants in the complex k_z plane. Also, improper (bottom Riemann sheet of the complex k_z plane) bound modes cannot be launched.

A *leaky mode* is a physical mode that presents *at least one* Floquet wavenumber within the visible region, or $\left|\beta_{z,p}\right| < k$ for some *p*. Taking into account of the physical condition in Sec. 2.3, and considering the harmonic in the first BZ, an observer along the positive *z*-direction would be reached by a radiating mode (excited at the origin) either when (i) it is improper and $0 < \beta_z < k$ and α_z is positive (forward mode), or when (ii) it is proper and $-k < \beta_z < 0$ and α_z is positive (backward mode).

Physical guided modes (leaky or bound) travel a long distance when the imaginary part of their wavenumber is small with respect to the host wavenumber, or $\alpha_z << k$.

3. NUMERICAL SIMULATION RESULTS: MODE DISPERSION DIAGRAMS

The aim of this section is the illustration of dispersion diagrams of linear chains of gold nanospheres, in the particular case of nanoparticles with radius $r = 25\,\text{nm}$ and center-to-center periodicity $d = 75\,\text{nm}$, embedded in free space (i.e., $\varepsilon_h = 1$).

The Drude parameters to model the permittivity of gold in (2) are taken from [26], adopted also in [27] regarding gold-dielectric nanoshells: $\omega_p = 1.36 \times 10^{16}$ rad/s, $\gamma = 1.05 \times 10^{14}$ s^{-1}, and $\varepsilon_\infty = 9.5$. These parameters have been chosen because the modeled permittivity $\varepsilon_m = \varepsilon' + i\varepsilon''$ agrees well with the experimental results presented in [28] by Johnson and Christy for a wide frequency range, as shown in Fig. 2.

The frequency range of interest for this paper is between 100 THz and 700 THz, which correspond to $kd/\pi = 0.05$ and $kd/\pi = 0.35$, respectively. Although the imaginary part is not perfectly modeled above 550 THz (as can be seen in Fig. 2(b)), the results will provide a trend for the modal dispersion diagrams of linear chains of gold nanospheres.

Dispersion diagrams are computed here for a chain of gold nanoparticles accounting also for metal losses. Specifically, if k_z is a complex wavenumber solution, then also $-k_z$ is a solution. In absence of losses, the correspondent complex conjugate $\pm k_z^*$ would be solutions as well. When losses are present, the complex conjugate solutions are modified from $\pm k_z^*$ correspondingly to the amount of losses introduced in the model. Here, the focus is on the wavenumber solutions belonging to the I and II quadrants of the complex k_z plane in the dispersion diagrams, i.e., those solutions with $\alpha_z \geq 0$, which are the only ones that can be captured in the path deformation described in Sec. 2.3 when observing

along the positive z axis. Note that this subset defines a complete set of modes in the linear chain because of the symmetry property stating that k_z and $-k_z$ are both solutions.
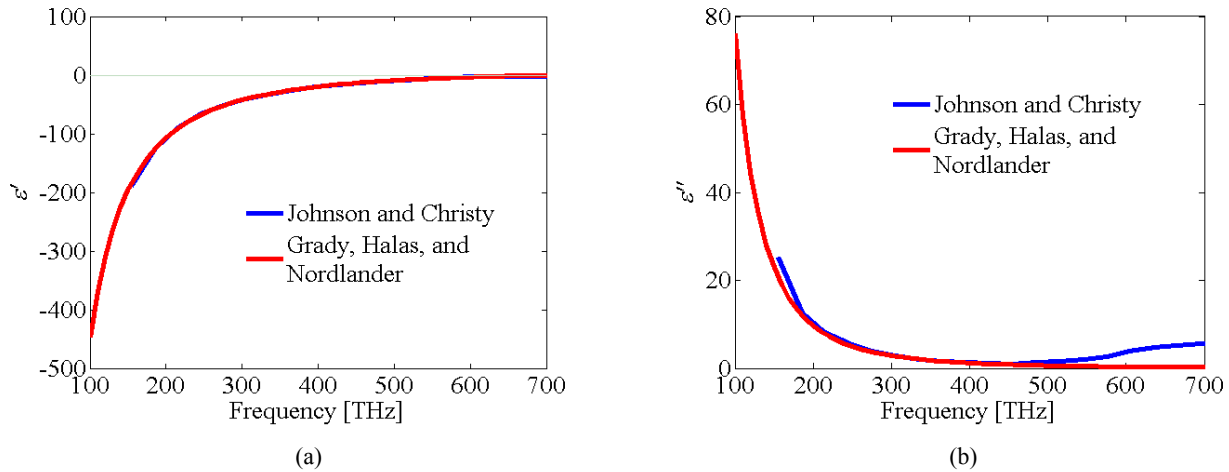

Fig. 2. Comparison of the (a) real and (b) imaginary parts of the gold complex permittivity between the chosen Drude model parameters provided by Grady, Halas, and Nordlander in [26] and the experimental results obtained by Johnson and Christy in [28].

3.1 Modes for transverse polarization

In this section, modal dispersion diagrams are shown for modes travelling along the z-direction polarized along x- or y-direction (transverse polarization, T-pol), in the case of gold nanospheres (accounting losses).

The dispersion diagrams for the real and imaginary parts of the wavenumber of each mode are reported in Figs. 3(a) and 3(b), respectively, whereas the evolution of the modes in the complex k_z plane varying frequency is presented in Fig. 5. Zoomed versions of the plots in Figs. 3 and 5 are reported in Figs. 4 and 6, respectively, for the sake of clarity.
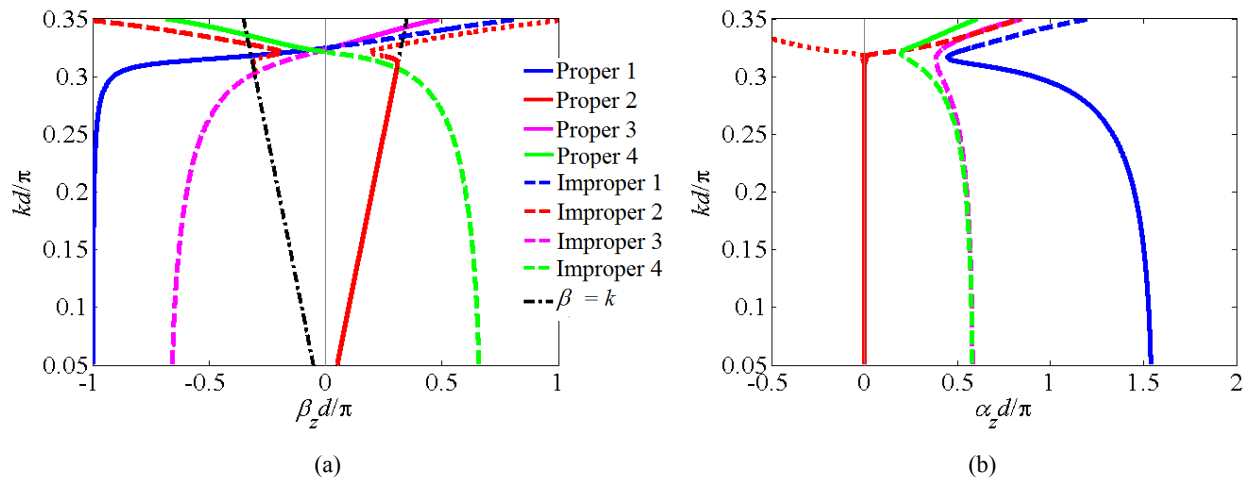

Fig. 3. Dispersion diagram for T-pol. (a) Real part and (b) imaginary part of the wavenumber $k_z = \beta_z + i\alpha_z$. Some modes with negative imaginary part are shown here (dotted lines). They are not captured in the path deformation described in Sec. 2.3; we include them here for the sake of showing how the modes in the I and II complex quadrants evolve when changing frequency.
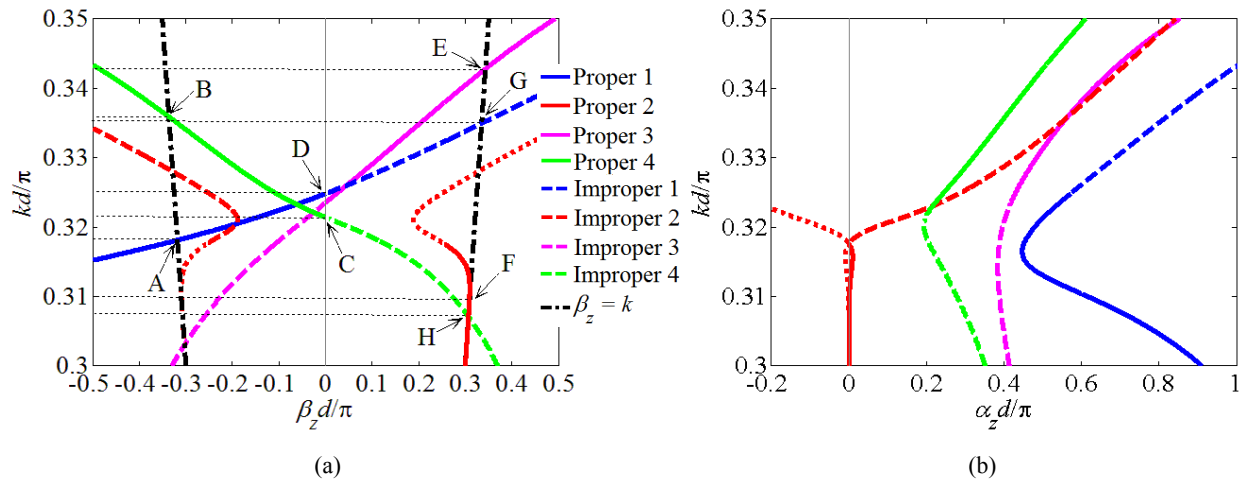
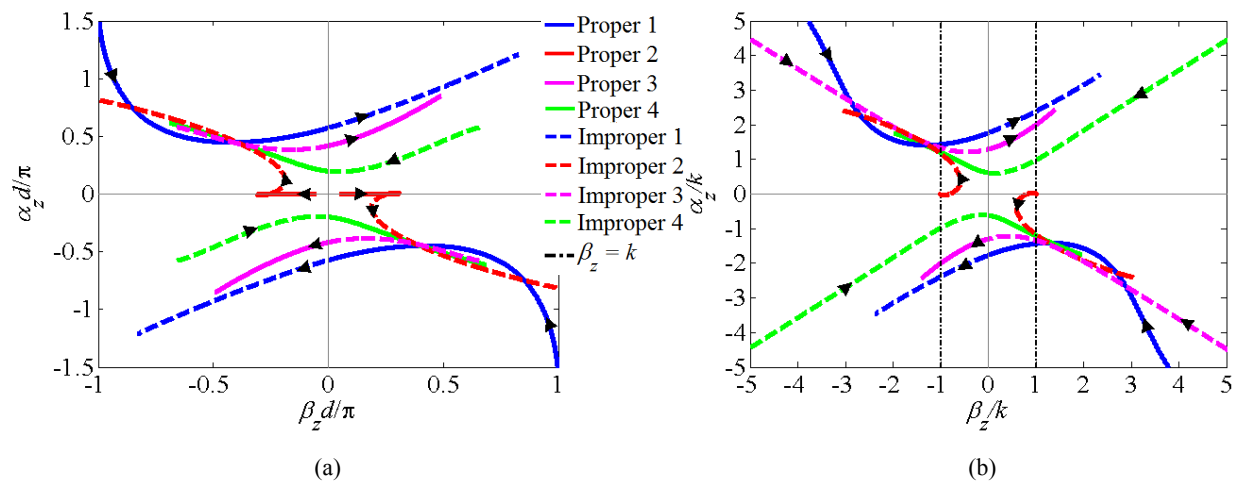Fig. 4. Zoom for the dispersion diagram for T-pol in Fig. 3.

Fig. 5. Modes in the complex k_z plane for T-pol, normalized with respect to (a) the period d, and (b) the host wavenumber k. Note that in (b), crossing "1" in the abscissa means crossing the light line. Arrows indicate direction of increasing frequency. Modes with negative imaginary part have a symmetric pattern with respect to those with positive imaginary part, and they are described with the same color scheme (and thus not shown as dotted lines, as was done in Figs. 3 and 4).

The physical bound modes for T-pol considering an observer along the positive z-direction are the following. The modes 'Proper 1' and 'Proper 4' in the II quadrant (Figs. 3(a) and 5(a)) are two bound backward modes; they do not have a small imaginary part with respect to the host wavenumber k, thus they cannot travel long distances from the excitation source. The bound mode 'Proper 1' can be excited for frequency values corresponding to kd/π smaller than the one in 'A' in Fig. 4(a) (for higher frequencies it becomes a proper leaky mode), whereas the bound mode 'Proper 4' can be excited for frequency values corresponding to kd/π higher than the one in 'B' in Fig. 4(a) (at lower frequencies this mode is a proper leaky one). The mode 'Proper 3' in the I quadrant is a bound forward mode; however, it has a quite large imaginary part, thus it decays very fast while travelling. It is physical only in the slow wave region, i.e., it can be excited for frequency values corresponding to kd/π higher than the one in 'E' in Fig. 4(a). The mode 'Proper 2' in the I quadrant is a bound forward mode for frequency values corresponding to kd/π smaller than the one in 'F' in Fig. 4(a), that has the real part of the wavenumber equal to the host wavenumber k (as can be seen in Fig. 3(a), this mode lies on top of the light line); indeed, this mode has a very small positive imaginary part in this frequency range, thus it can travel very long distances from the excitation source.

The physical leaky modes for T-pol considering an observer along the positive z-direction are the following. The modes 'Improper 1' and 'Improper 4', for frequency values corresponding to kd/π between 'D' and 'G', and between 'H' and 'C' in Fig. 4(a), respectively, are radiating forward leaky modes. The 'Improper 1' does not have a small imaginary part with respect to the host wavenumber k, and thus cannot be used as a directive radiator. However, the dashed green ('Improper 4') has a smaller imaginary part than the dashed blue one, near the leaky region $\beta_z \approx 0$, and thus it could be used for radiation. The modes 'Proper 1' and 'Proper 4' in the II quadrant, for frequency values corresponding to kd/π between 'A' and 'D', and between 'C' and 'B' in Fig. 4(a), respectively, are two radiating backward leaky modes. Again, the 'Proper 1' (solid blue) does not have a small imaginary part. However, the solid green ('Proper 4') has a smaller imaginary part than the blue one, near the leaky region $\beta_z \approx 0$, and thus it could be used for moderate directive radiation.

The plots shown in Fig. 5 provide a complete picture of the evolution of the modes for T-pol by varying frequency in the complex k_z plane. They also clarify what it has been previously stated about the definition of the physical bound and leaky waves. One can observe the total symmetry with respect to the origin. A zoom is provided in Fig. 6.
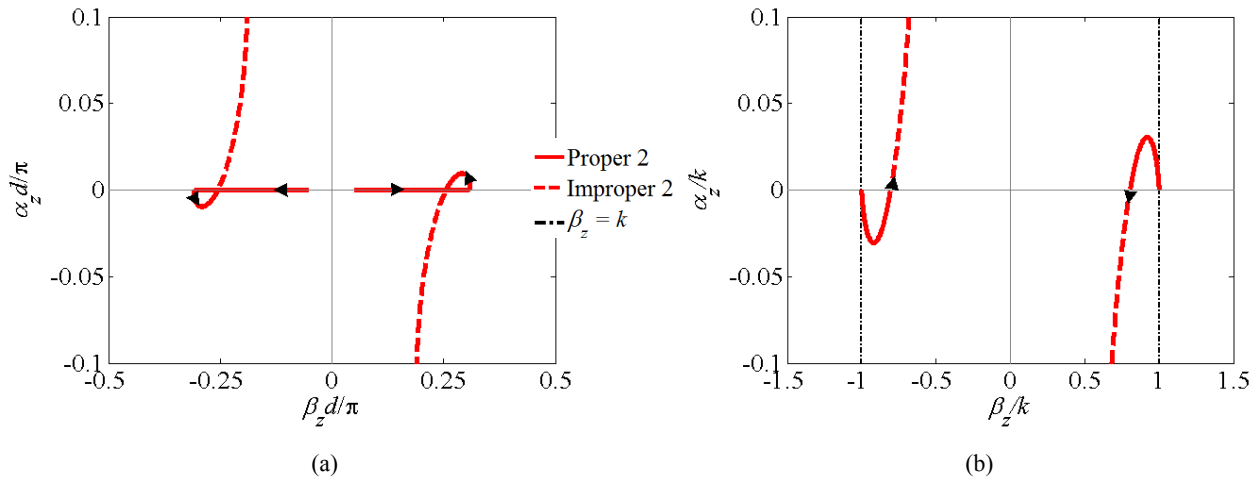

Fig. 6. Zoom for the complex k_z plane for T-pol in Fig. 5.

For the sake of clarity, we show in Fig. 7 only the subset of the excitable modes (bound and leaky) for transverse polarization, assuming an observer along the positive z axis and, for instance, a source near the origin.
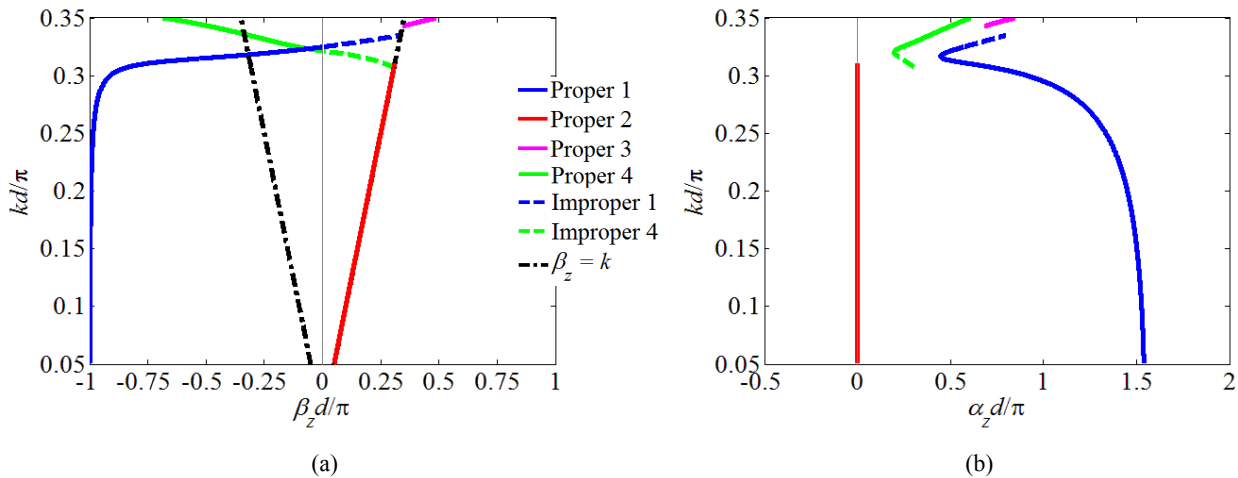

Fig. 7. As in Fig. 3, showing only the subset of physical modes (for an observer located on the positive z axis, and a source near the origin, for instance).

3.2 Modes for longitudinal polarization

In this section, dispersion diagrams are shown for modes travelling along the z-direction polarized along z (longitudinal polarization, L-pol), in the case of lossy gold nanospheres.

As in Sec. 3.1, the dispersion diagrams for the real and imaginary parts of the wavenumber of each mode are reported in Figs. 8(a) and 8(b), respectively, with a zoom in Fig. 9 for clarity, whereas the evolution of the modes in the complex k_z plane varying frequency is presented in Fig. 10.

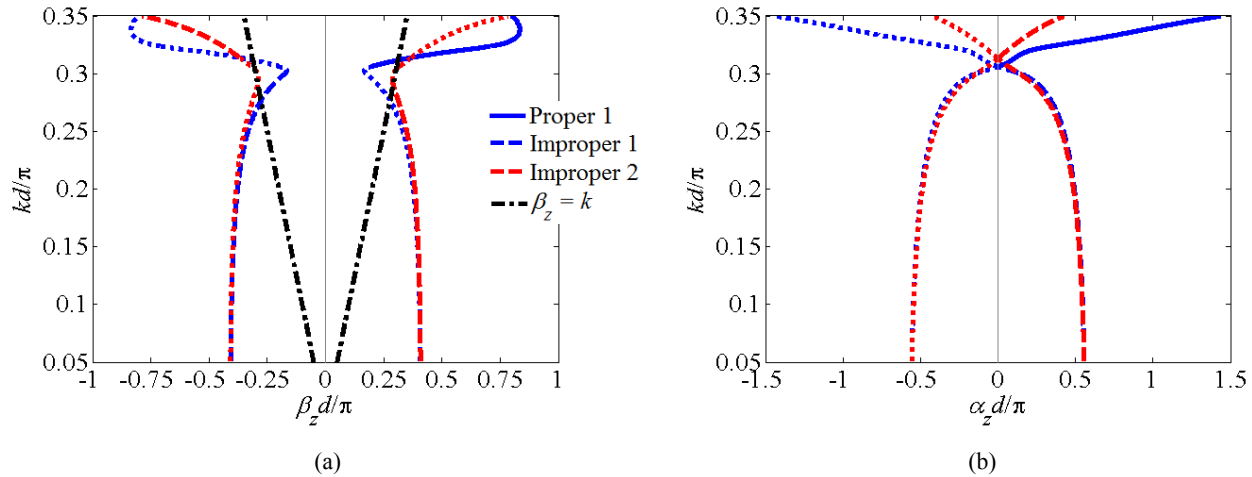(a)   (b)

Fig. 8. Dispersion diagram for L-pol. (a) Real part and (b) imaginary part of the wavenumber $k_z = \beta_z + i\alpha_z$.
Modes with negative imaginary part are shown here (dotted lines). They are not captured in the path deformation described in Sec. 2.3; we include them here for the sake of showing how the modes in the I and II complex quadrants evolve when changing frequency.
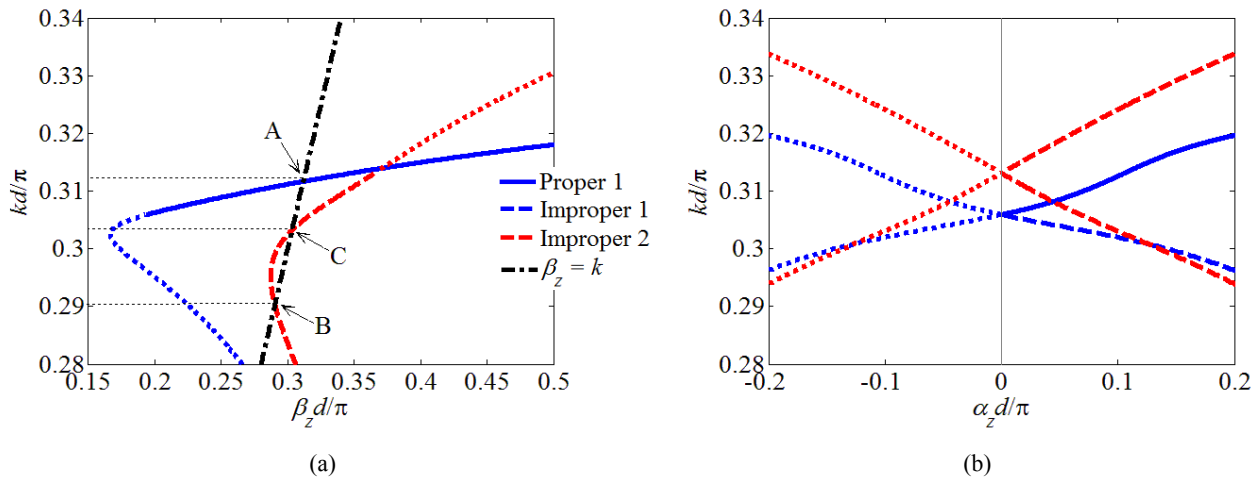

(a)   (b)

Fig. 9. Zoom for the dispersion diagram for L-pol in Fig. 8.

The physical bound modes for L-pol considering an observer along the positive z-direction are the following. The mode 'Proper 1' is a bound forward mode; it has a small imaginary part when it is close to the light line in the $k\beta$-plane, as it can be noticed from the zoom provided in Fig. 9, thus it can travel long distances from the excitation source with small decay. This mode can be excited for frequency values corresponding to kd/π higher than the one in 'A' in Fig. 9(a).

The physical leaky modes for L-pol considering an observer along the positive z-direction and, for instance, a source in proximity of the origin, are the following. The mode 'Improper 2' is a radiating forward mode for frequency values

corresponding to kd/π between 'B' and 'C' in Fig. 9(a). It has a small imaginary part with respect to the host wavenumber k, as it can be noticed again from the zoom provided in Fig. 9. However, notice that this mode lies very close to the light line, as can be easily observed in Fig. 10(b); since the dipoles approximating the nanospheres are longitudinally polarized (i.e., along the z-direction), their far-field radiation pattern would behave with classical $\sin(\theta)$ shape, with a far field null corresponding to the direction along which the dipoles are aligned. Indeed, in the case of the analyzed linear chain, when $\beta_z = k$ the radiation should take place along the z-direction; this is not possible due to the aforementioned null, present when the structure has finite size; whereas, when $\beta_z < k$ for $\beta_z \approx k$, a very small radiation (due to the dipolar sinusoidal far-field behavior) could take place.
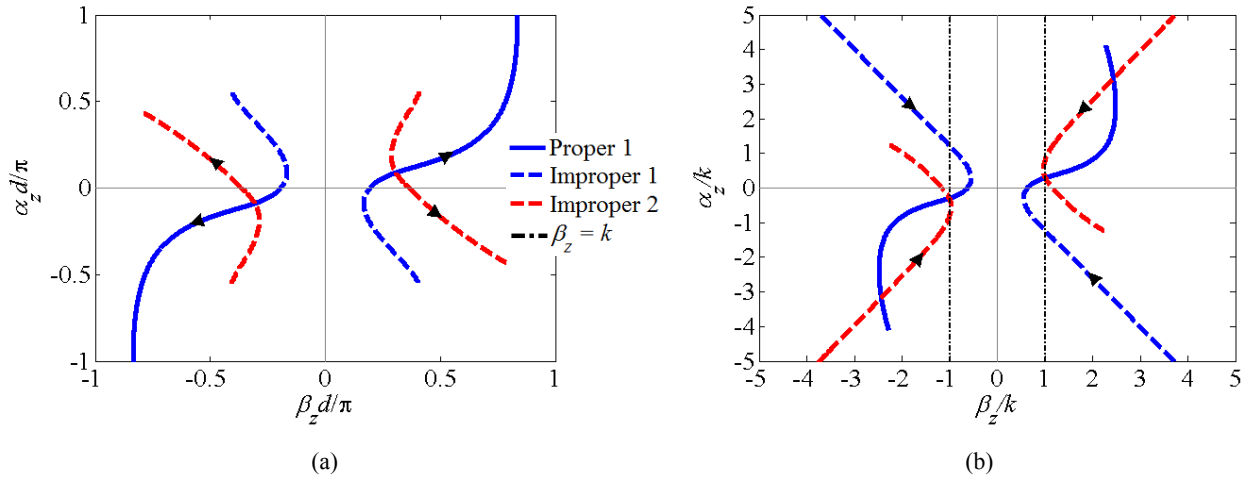

Fig. 10. Modes in the complex relative k_z plane for L-pol, normalized with respect to (a) the period d, and (b) the host wavenumber k. Note that in (b), crossing "1" in the abscissa means crossing the light line. Arrows indicate direction of increasing frequency. Modes with negative imaginary part have a symmetric pattern with respect to those with positive imaginary part, and they are described with the same color scheme (and thus not shown as dotted lines, as was done in Figs. 8 and 9).

The plots shown in Fig. 10 provide a complete picture of the evolution of the modes for L-pol by varying frequency in the complex k_z plane. They also clarify what it has been previously stated about the definition of the physical bound and leaky waves.
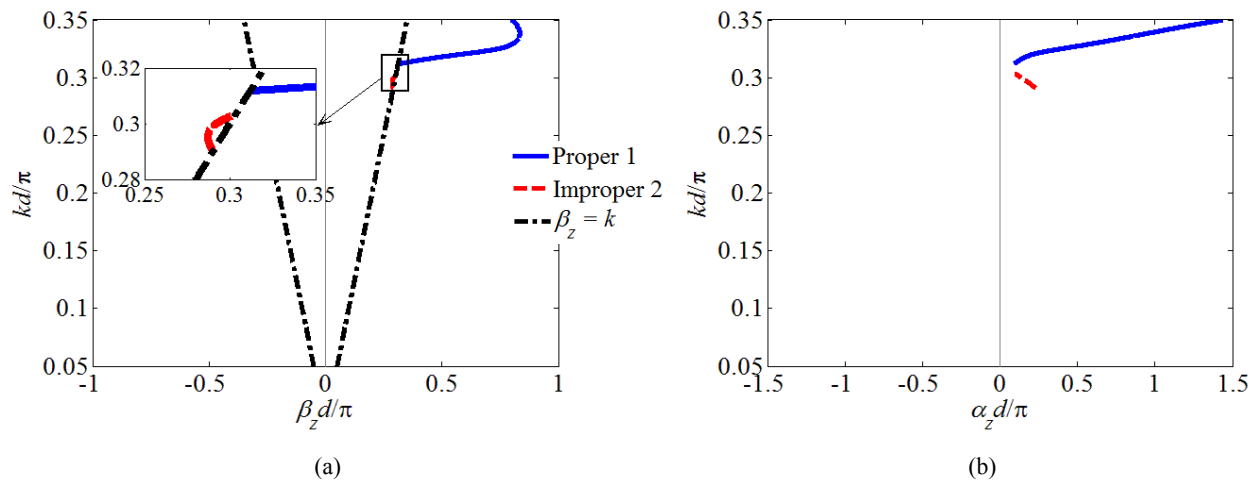

Fig. 11. As in Fig. 8, showing only the subset of physical modes (for an observer located on the positive z axis, and a source near the origin, for instance).

For the sake of clarity, we show in Fig. 11 only the subset of excitable modes (physical bound and leaky modes) for longitudinal polarization, assuming an observer along the positive z axis and, for instance, a source near the origin.

4. CONCLUSION

In this work, modal dispersion diagrams, i.e., wavenumber versus frequency, have been computed for modes traveling in a periodic linear array (a chain) of gold nanospheres. The single dipole approximation has been adopted to model the behavior of each nanoparticle at optical frequencies, which is a good approximation when working close to the plasma resonance frequency of the nanospheres; however, more accurate results, for small period comparable with the spheres' radius, would involve multipole field contributions. Physical and nonphysical modes in a chain have been described in this work. This is the first time such a complete physical characterization in a chain of gold nanoparticles has been presented.

REFERENCES

[1]   P. Alitalo, C. Simovski, A. Viitanen *et al.*, "Near-field enhancement and subwavelength imaging in the optical region using a pair of two-dimensional arrays of metal nanospheres," *Physical Review B,* 74(23), 235425 (2006).
[2]   S. Steshenko, F. Capolino, S. A. Tretyakov *et al.*, "Super-Resolution and Near-Field Enhancement with Layers of Resonant Arrays of Nanoparticles," Chapter 4 in *Applications of Metamaterials*, F. Capolino, Ed., p. 4.1, CRC Press, Boca Raton, FL (2009).
[3]   C. R. Simovski, A. J. Viitanen, and S. A. Tretyakov, "Sub-wavelength imaging and resolution by two linear chains of plasmonic particles," *IEEE Antennas and Propagation Society International Symposium, Honolulu, HI,*. 4344-4347 (2008).
[4]   C. R. Simovski, A. J. Viitanen, and S. A. Tretyakov, "Sub-wavelength resolution in linear arrays of plasmonic particles," *Journal of Applied Physics,* 101(12), 123102 (2007).
[5]   C. R. Simovski, S. A. Tretyakov, and A. J. Viitanen, "Subwavelength imaging in a superlens of plasmon nanospheres," *Technical Physics Letters,* 33(3), 264-266 (2007).
[6]   A. F. Koenderink, "Plasmon Nanoparticle Array Waveguides for Single Photon and Single Plasmon Sources," *Nano Letters,* 9(12), 4228-4233 (2009).
[7]   F. Liu, Z. Cao, C. Tang *et al.*, "Ultrathin Diamond-like Carbon Film Coated Silver Nanoparticles-Based Substrates for Surface-Enhanced Raman Spectroscopy," *ACS Nano,* 4(5), 2643-2648 (2010).
[8]   J. Beermann, S. M. Novikov, K. Leosson *et al.*, "Surface enhanced Raman imaging: periodic arrays and individual metal nanoparticles," *Optics Express,* 17(15), 12698-12705 (2009).
[9]   I. Firkowska, S. Giannona, J. A. Rojas-Chapana *et al.*, "Biocompatible Nanomaterials and Nanodevices Promising for Biomedical Applications ", in *Nanomaterials for Application in Medicine and Biology*, M. Giersig and G. B. Khomutov, Eds., p. I.1, Springer, Berlin (2008).
[10] A. J. Haes, and R. P. Van Duyne, "A nanoscale optical biosensor: Sensitivity and selectivity of an approach based on the localized surface plasmon resonance spectroscopy of triangular silver nanoparticles," *Journal of the American Chemical Society,* 124(35), 10596-10604 (2002).
[11] I. E. Sendroiu, and R. M. Corn, "Nanoparticle diffraction gratings for DNA detection on photopatterned glass substrates," *Biointerphases,* 3(3), FD23-FD29 (2008).
[12] S. Campione, S. Steshenko, and F. Capolino, "Complex bound and leaky modes in chains of plasmonic nanospheres," to be submitted to *Optics Express*, (2011).
[13] S. Campione, and F. Capolino, "Linear and Planar Periodic Arrays of Metallic Nanospheres: Fabrication, Optical Properties and Applications," in *Selected Topics in Metamaterials and Photonic Crystals*, A. Andreone, A. Cusano, A. Cutolo *et al.*, Eds., World Scientific Publishing, Hackensack, NJ (in print, 2011).
[14] F. Capolino, D. R. Jackson, and D. R. Wilton, "Field Representations in Periodic Artificial Materials Excited by a Source," Chapter 12 in *Theory and Phenomena of Metamaterials*, F. Capolino, Ed., p. 12.1, CRC Press, Boca Raton, FL (2009).
[15] S. Steshenko, and F. Capolino, "Single Dipole Approximation for Modeling Collections of Nanoscatterers," Chapter 8 in *Theory and Phenomena of Metamaterials*, F. Capolino, Ed., p. 8.1, CRC Press, Boca Raton, FL (2009).
[16] C. F. Bohren, and D. R. Huffman, *Absorption and Scattering of Light by Small Particles*, Wiley, New York (1983).

[17] A. Sihvola, "Mixing Rules," Chapter 9 in *Theory and Phenomena of Metamaterials*, F. Capolino, Ed., p. 9.1, CRC Press, Boca Raton, FL (2009).

[18] A. Sihvola, "Polarizability of Simple-Shaped Particles," Chapter 7 in *Theory and Phenomena of Metamaterials*, F. Capolino, Ed., p. 7.1, CRC Press, Boca Raton, FL (2009).

[19] R. Ruppin, "Evaluation of extended Maxwell-Garnett theories," *Optics Communications,* 182(4-6), 273-279 (2000).

[20] W. T. Doyle, "Optical properties of a suspension of metal spheres," *Physical Review B,* 39(14), 9852 (1989).

[21] V. R. Komanduri, F. Capolino, D. R. Jackson *et al.*, "Computation of the one-dimensional free-space periodic green's function for leaky waves using the ewald method," *Proceedings URSI General Assembly, Chicago, IL.*

[22] F. T. Celepcikay, D. R. Wilton, D. R. Jackson *et al.*, "Choosing splitting parameters and summation limits in the numerical evaluation of 1-D and 2-D periodic Green's functions using the Ewald method," *Radio Science,* 43(6), RS6S01 (2008).

[23] F. Capolino, D. R. Wilton, and W. A. Johnson, "Efficient computation of the 3D Green's function for the Helmholtz operator for a linear array of point sources using the Ewald method," *Journal of Computational Physics,* 223(1), 250-261 (2007).

[24] P. Baccarelli, S. Paulotto, and C. Di Nallo, "Full-wave analysis of bound and leaky modes propagating along 2D periodic printed structures with arbitrary metallisation in the unit cell," *IET Microwaves, Antennas & Propagation,* 1(1), 217-225 (2007).

[25] A. L. Fructos, S. Campione, F. Capolino *et al.*, "Characterization of complex plasmonic modes in 2D-periodic arrays of metal nanospheres," to be submitted to *Journal of the Optical Society of America B*, (2011).

[26] N. K. Grady, N. J. Halas, and P. Nordlander, "Influence of dielectric function properties on the optical response of plasmon resonant metallic nanoparticles," *Chemical Physics Letters,* 399(1-3), 167-171 (2004).

[27] S. Campione, A. Vallecchi, and F. Capolino, "Closed form formulas and tunability of resonances in pairs of gold-dielectric nanoshells," *Proceedings of the SPIE - The International Society for Optical Engineering,* 7757, 775738 (2010).

[28] P. B. Johnson, and R. W. Christy, "Optical Constants of the Noble Metals," *Physical Review B,* 6(12), 4370 (1972).